

# Four-coloring model and frustrated superfluidity in the diamond lattice

Gia-Wei Chern<sup>1,2</sup> and Congjun Wu<sup>3</sup>

<sup>1</sup>*Department of Physics, University of Wisconsin, Madison, WI 53706, USA*

<sup>2</sup>*Theoretical Division, Los Alamos National Laboratory, Los Alamos, NM 87545, USA*

<sup>3</sup>*Department of Physics, University of California, San Diego, CA 92093, USA*

We propose a novel four-coloring model which describes “frustrated superfluidity” of  $p$ -band bosons in the diamond optical lattice. The superfluid phases of the condensate wavefunction on the diamond-lattice bonds are mapped to four distinct colors with the constraint that four differently colored bonds meet at the same site. We show that the combined effects of strong intra-site repulsions, inter-site phase coherence, and anisotropy give rise to a macroscopically degenerate ground state at the classical level. By further mapping the problem to an antiferromagnetic Potts model on the pyrochlore lattice, we demonstrate that both color and orbital angular momentum correlations exhibit power-law decay in the degenerate manifold that is described by an emergent magnetostatic theory with three independent flux fields.

PACS numbers: 03.75.Ss, 05.50.+q, 71.10.Fd, 73.43.Nq

Strongly frustrated systems are hosts to various complex orders, unusual phases and elementary excitations. A well-studied example is the emergence of a critical Coulomb phase in systems ranging from water ice [1], pyrochlore magnets (spin ice) [2, 3] to  $p$ -band fermions in the optical diamond lattice (orbital ice) [4]. A ubiquitous feature here is the appearance of an extensively degenerate manifold due to a large number of unconstrained degrees of freedom. Although the macroscopic degeneracy is usually of geometrical origin, especially for magnetic systems [5], the nontrivial spatial dependence of anisotropic orbital interactions in optical lattices provides a new playground for studying interesting phenomena related to a highly degenerate manifold [4, 6–8]. In particular, for  $p$ -orbital bosonic condensates in optical lattices, the frustrated couplings between the  $U(1)$  phase degrees of freedom can lead to intriguing quantum many-body states [9, 10].

For conventional superfluid states of bosons, their ground state wavefunctions are positive-definite as stated by the “no-node” theorem which is valid under very general conditions [11]. It means that the superfluid phases are uniform over the entire condensate, in other words, non-frustrated. Exotic states of bosons beyond the “no-node” theorem have been theoretically proposed and experimentally realized in ultra-cold atom optical lattices [12]. For example, when bosons are pumped to high orbital bands, their condensate wavefunctions form non-trivial representations of the lattice symmetry group, dubbed “unconventional” Bose-Einstein condensations, say, the complex-valued  $p + ip$ -type condensates with spontaneously broken time-reversal symmetry (see Ref. [9] for a brief review). These condensates are metastable excited states, and hence are not constrained by the “no-node” theorem.

In this article we study the Bose-Einstein condensates formed by bosons pumped into the  $p$ -orbital bands in a diamond lattice. We show that the problem of inter-

site phase coherence in this lattice represents a highly frustrated system and can be mapped to a four-coloring model on the diamond lattice. By combining analytical arguments and numerical simulations, we demonstrate the existence of an algebraic Coulomb phase in the highly degenerate ground state of the diamond-lattice 4-coloring model. Our work thus provides a three-dimensional (3D) generalization of the celebrated three-coloring model on the planar honeycomb lattice [13], and a similar 4-coloring problem on the square lattice [14]. In both cases the ground state is extensively degenerate and exhibits power-law color correlations.

*Model Hamiltonian.* We begin with a discussion of the Hamiltonian for  $p$ -orbital bosons in the diamond optical lattice. This bipartite lattice can be generated by the interference of four laser beams with suitably arranged light polarizations as discussed in Ref. [15]. The unit vectors from each site in sublattice  $A$  to its four neighboring  $B$ -sites are denoted as  $\hat{\mathbf{n}}_0 = [111]$ ,  $\hat{\mathbf{n}}_1 = [1\bar{1}\bar{1}]$ ,  $\hat{\mathbf{n}}_2 = [\bar{1}1\bar{1}]$ , and  $\hat{\mathbf{n}}_3 = [\bar{1}\bar{1}1]$ . Around the center of each lattice site, the point group symmetry is  $T_d$  of which the degenerate  $p_{x,y,z}$ -orbitals form a triplet irreducible representation. The band energy is thus represented as

$$H_0 = t_{\parallel} \sum_{\nu=0}^3 \sum_{\langle ij \rangle \parallel \hat{\mathbf{n}}_{\nu}} \left\{ p_{i,\nu}^{\dagger} p_{j,\nu} + \text{h.c.} \right\}, \quad (1)$$

where  $p_{\nu}$  is the projection of the  $p$ -orbitals along the direction of  $\hat{\mathbf{n}}_{\nu}$ :  $p_{\nu} = p_x \hat{n}_{\nu}^x + p_y \hat{n}_{\nu}^y + p_z \hat{n}_{\nu}^z$ . We only keep the longitudinal hopping between  $p$ -orbitals along the bond direction, *i.e.*, the  $\sigma$ -bonding, and neglect the small transverse hopping terms. Here  $t_{\parallel}$  is positive because of the odd parity of  $p$ -orbitals.

The general on-site interaction has the form:  $H_{\text{int}} = \sum_i V_{ab;cd} p_{i,a}^{\dagger} p_{i,b}^{\dagger} p_{i,c} p_{i,d}$ , where  $V_{ab;cd} = g \int d^3\mathbf{r} \psi_a(\mathbf{r}) \psi_b(\mathbf{r}) \psi_c(\mathbf{r}) \psi_d(\mathbf{r})$ ,  $g$  is the contact interaction parameter, and  $\psi_a$  ( $a = x, y, z$ ) are Wannier functions of  $p$ -orbitals. The  $T_d$  group contains the symmetry

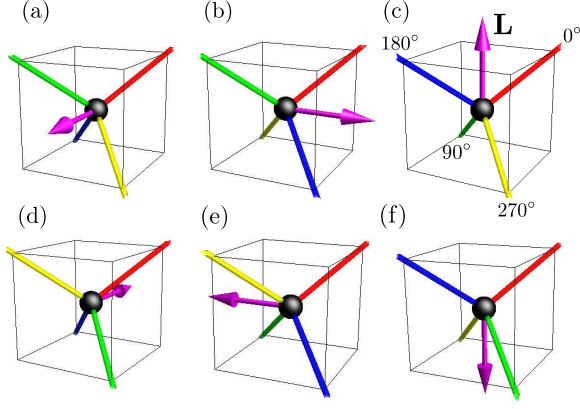


FIG. 1: (Color online) Mapping between the orbital angular momentum and color configuration on the diamond lattice. The red, green, blue, and yellow bonds have phases  $\phi = 0^\circ, 90^\circ, 180^\circ$ , and  $270^\circ$ , respectively, when projected to the base plane perpendicular the direction of angular momentum  $\mathbf{L}$ . The mapping is not one-to-one, as each  $\mathbf{L}$  corresponds to 4 different cyclic permutations of the colors which preserve the same chirality.

of rotation around the  $z$ -axis followed by the inversion, which transforms  $\psi_z \rightarrow -\psi_z, \psi_x \rightarrow -\psi_y$ , and  $\psi_y \rightarrow \psi_x$ . Since  $V_{ab;cd}$  should be invariant under this transformation, symmetry consideration indicates that there are only two independent parameters  $V_{xx;xx}$  and  $V_{xy;xy}$ . The interaction terms can thus be reorganized as

$$H_{\text{int}} = U \sum_i \left\{ n_i^2 - \frac{1}{3} \mathbf{L}_i^2 \right\} + \Delta U \sum_i \sum_{\alpha=x,y,z} n_{i,\alpha}^2, \quad (2)$$

where  $n_{i,\alpha}$  is the particle number in  $p_\alpha$ -orbital ( $\alpha = x, y, z$ ) at site  $\mathbf{r}_i$ ,  $n_i = n_{i,x} + n_{i,y} + n_{i,z}$ , and  $L_i^\mu = -\frac{i}{2} \epsilon_{\mu\nu\lambda} p_\nu^\dagger p_\lambda$  is the orbital angular momentum operator. The first term in Eq. (2) represents the Hubbard interaction with the spherical symmetry around the site center and  $U = 3V_{xy,xy}$  as given in Ref. [9, 16]. We assume repulsive interactions  $U > 0$ . The ferro-orbital interaction means that bosons prefer to maximize the on-site orbital angular momentum such that their wavefunctions are most extended spatially to reduce the onsite repulsion [9], analogous to the second Hund's rule of electrons filling in degenerate atomic orbitals. The second term with  $\Delta U = \frac{1}{2}(V_{xx;xx} - 3V_{xy,xy})$  comes from the  $T_d$  symmetry crystal field. Compared with the spherically symmetric case ( $\Delta U = 0$ ), the angular distributions of Wannier orbitals  $\psi_a$  in the diamond lattice expand from  $\pm\hat{\mathbf{x}}, \pm\hat{\mathbf{y}}, \pm\hat{\mathbf{z}}$  toward the the bond directions  $\hat{\mathbf{n}}_\nu$ . This enhances the inter-orbital repulsion but weakens the intra-orbital one, such that  $\Delta U < 0$ .

*Mapping to the 4-coloring model.* We consider the strong coupling limit with a weak crystal field, *i.e.*,  $U \gg t_\parallel$  and  $U \gg |\Delta U|$ . Assuming that the average filling is large, we approximate each site as a small condensate

and treat it classically. In order to minimize the  $U$ -term, bosons condense into the orbital of  $[p^\dagger(\hat{\mathbf{e}}_1) + i p^\dagger(\hat{\mathbf{e}}_2)]/\sqrt{2}$  with  $\hat{\mathbf{e}}_1 \perp \hat{\mathbf{e}}_2$  at each site, where  $p^\dagger(\hat{\mathbf{e}}_i)$  is the projection of the  $p$ -orbitals on the direction of  $\hat{\mathbf{e}}_i$ . The corresponding angular momentum is  $\mathbf{L} \parallel \hat{\mathbf{e}}_1 \times \hat{\mathbf{e}}_2$ .

The crystal field from a  $\Delta U < 0$  term aligns  $\mathbf{L}$  to directions along  $\pm\hat{\mathbf{x}}, \pm\hat{\mathbf{y}}, \pm\hat{\mathbf{z}}$ . Assuming the average filling per site is  $n$  and neglecting the quantum depleting of the condensation fraction, the kinetic energy of each nearest-neighbor bond becomes

$$E_{ij} = -\frac{2}{3} n t_\parallel \cos(\phi_{i,\nu} - \phi_{j,\nu}), \quad (3)$$

where  $\langle ij \rangle \parallel \hat{\mathbf{n}}_\nu$ ,  $\phi_{i,\nu}$  is the superfluid phase along bond  $\langle ij \rangle$  at site  $\mathbf{r}_i$ , and the factor  $\frac{2}{3}$  comes from the angles between the bond direction  $\hat{\mathbf{n}}_\nu$  and the base planes of  $\hat{\mathbf{e}}_{1,2}$  for  $\mathbf{L}_i$  at site  $i$  and  $\mathbf{L}_j$  at site  $j$ , respectively. The  $U(1)$  phase in each site winds  $2\pi$  around the nodal line which is parallel to  $\mathbf{L}_i$ .

The phase  $\phi_{i,\nu}$  along the bond direction  $\hat{\mathbf{n}}_\nu$  is the same as that along the projection of  $\hat{\mathbf{n}}_\nu$  in the  $\hat{\mathbf{e}}_{1,2}$  plane; see Fig. 1. For  $\Delta U < 0$ , the  $\hat{\mathbf{e}}_{1,2}$  plane is perpendicular to one of the cubic axes. Since the projections of the four  $\hat{\mathbf{n}}_\nu$  in the  $xy, yz$  and  $zx$  planes are evenly distributed,  $\phi_{i,\nu}$  take values of  $\sigma_{ij} \frac{\pi}{2}$  up to an overall  $U(1)$  phase, where  $\sigma_{ij} = 0, 1, 2, 3$  defines the color indices for the bond  $\langle ij \rangle \parallel \hat{\mathbf{n}}_\nu$ . They correspond to colors **R**, **G**, **B**, and **Y**, respectively, in Fig. 1. We can thus express  $\phi_{i,\nu}$  as

$$\phi_{i,\nu} = \theta_i + \sigma_{ij} \frac{\pi}{2}, \quad (4)$$

where  $\theta_i$  denotes the  $U(1)$  phase fluctuation. The constraint of phase coherence is that each bond can only be assigned with one color and four bonds connecting each site take different colors (Fig. 1).

To minimize the kinetic energy, we freeze  $\theta_i = 0$  for all sites, such that  $\phi_{i,\nu} = \phi_{j,\nu}$  for each bond. The classic ground states of the  $p$ -band bosons thus map into a highly frustrated 4-coloring model. An example of such configurations in the diamond lattice is shown in Fig. 2. There are  $4! = 24$  coloring configurations on each site  $i$ , and 6 different orientations ( $\pm\hat{\mathbf{x}}, \pm\hat{\mathbf{y}}, \pm\hat{\mathbf{z}}$ ) for  $\mathbf{L}_i$ , which are defined as “chirality” of the condensate. For each chirality, there are  $24/6 = 4$  coloring configurations corresponding to a  $C_4$  rotation around the direction of  $\mathbf{L}_i$ ; see Fig. 1. Consequently, the classical ground states correspond to those of the 4-coloring model modular 4. The chirality can be explicitly computed as  $\mathbf{L}_i \parallel (\hat{\mathbf{n}}_{\frac{\pi}{2}} - \hat{\mathbf{n}}_0) \times (\hat{\mathbf{n}}_\pi - \hat{\mathbf{n}}_{\frac{3\pi}{2}})$ , where  $\hat{\mathbf{n}}_\varphi$  denotes the bond with phase  $\varphi$  at site  $\mathbf{r}_i$ .

The phase correlation of the  $p$ -band condensate has contributions from both the discrete color variables  $\sigma_{ij}$  and the  $U(1)$  variables  $\theta_i$ . At the classic level, it is dominated by the color correlations at low temperatures in which the gapped excitations of defects can be neglected. For all the defect-free configurations, the partition functions for thermal phase fluctuations are identical, and

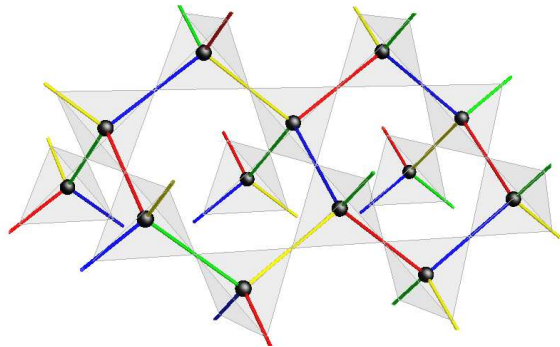


FIG. 2: (Color online) Coloring of the diamond lattice that satisfy the constraints that four bonds attached to the same vertex have different colors. By assigning a 4-state Potts variable to label the coloring of the bond, the 4-coloring model on the diamond lattice can be mapped to an antiferromagnetic Potts model on its medial pyrochlore lattice.

thus the color correlations of  $\sigma_{ij}$  and phase fluctuations of  $\theta_i$  are decoupled. In 3D below a critical temperature  $T_c$ , there exists a long-range-order for the  $U(1)$  phase  $\theta_i$ , thus up to a temperature-dependent factor, the correlations of  $\phi_{i,\nu}$  are just described by the color correlations. However, quantum phase fluctuations may select an optimal coloring pattern through the “order by disorder” mechanism, which should occur at a very low temperature scale  $T'_c$ . Thus the 4-coloring model applies at  $T'_c \ll T \ll T_c$ , and we will see that algebraic phase correlation develops in this temperature regime.

*Antiferromagnetic Potts model on pyrochlore lattice.* Since the color variables are defined on bonds of the diamond lattice, it is more convenient to consider an equivalent Potts model in the pyrochlore lattice whose sites correspond to the bond midpoints in the diamond lattice (Fig. 2). A Potts variable  $\sigma_m = \sigma_{ij} = 0, 1, 2, 3$  is assigned to each pyrochlore site such that the corresponding phase is given by Eq. (4). The constraint that bonds attached to the same vertex have different colors translates to an antiferromagnetic interaction between nearest-neighbor Potts variables on the pyrochlore:

$$H = J \sum_{\langle ml \rangle} \delta(\sigma_m, \sigma_l), \quad (5)$$

Here the coupling constant  $J \sim nt_{\parallel}$ . To avoid confusion, we use  $m, l$  to label the pyrochlore sites. The hard constraint of the 4-coloring model is recovered in the  $J \rightarrow \infty$  limit. Consider first a single tetrahedron, there are  $4! = 24$  ground states in which the four sites are in different Potts states. These correspond to the 24 coloring schemes on a diamond site. When generalizing to the pyrochlore lattice, model (5) represents an under-constrained system with an extensively degenerate ground state, similar to their two-dimensional counterparts [13, 14].

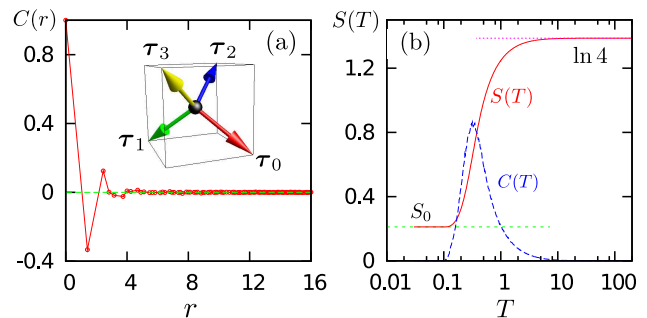


FIG. 3: (Color online) (a) The angular averaged color correlation function  $C(r)$  on a system with linear size  $L = 10$  in the ground state of the pyrochlore 4-state Potts model. The inset shows the four unit vectors  $\tau_\nu$  ( $\nu = 0 \sim 3$ ) corresponding to the four different colors. (b) Entropy  $S$  and specific heat  $C$  as a function of temperature  $T$  obtained from the Monte Carlo simulations. The energy is measured in units of  $J'$ . The entropy  $S(T)$  is obtained by numerically integrating the specific heat curve; the integration constant  $S_0 = 0.2112$ .

In order to determine the structure of the degenerate manifold, we employ Monte Carlo simulations with non-local loop updates on a finite lattice. In each loop update, two sites are chosen randomly in a given ground state. These two sites will necessarily be of different color, say **R** and **B**. With periodic boundary conditions, a **RB**-colored loop containing the two chosen sites is uniquely determined. By exchanging colors **R** and **B** over the length of the loop, the non-local update results in a new ground state as all the color constraints remain satisfied. There are a total of  $\binom{4}{2} = 6$  types of loops with different colors. Since all the microstates have equal statistical weight, loop updates of all lengths and colors are accepted in order to satisfy detailed balance.

We first study the color correlations in the ground state. To this end, we introduce four unit vectors  $\tau_\nu$  pointing toward different corners of a regular tetrahedron as shown in the inset of Fig. 3(a). The correlation function between two sites is defined as  $C(r_{ml}) = \langle \tau_{\sigma_m} \cdot \tau_{\sigma_l} \rangle$ , which equals 1 for  $\sigma_m = \sigma_l$  and  $-1/3$  for  $\sigma_m \neq \sigma_l$ . Fig. 3(a) shows the color correlation averaged over different angular directions obtained from Monte Carlo simulations. The correlations  $C(r)$  fall off rapidly beyond a few nearest-neighbor distances, indicating a color-disordered ground state.

The degeneracy of the ground state can be computed by a method similar to the Pauling estimation for the degeneracy of water ice [1]. Consider a single tetrahedron,  $4!$  out of  $4^4$  Potts configurations satisfy the color constraint. Treating the constraints imposed by different tetrahedra as independent, the number of degenerate ground states is  $W \sim 4^N (4!/4^4)^{N/2}$ , where  $N$  is the number of pyrochlore sites and  $N/2$  is the number of tetrahedra (or diamond sites). This estimation gives an entropy:  $S_0/Nk_B = (1/2) \ln(3/2) \approx 0.2027$ . The residual entropy

can also be estimated with the aid of Monte Carlo simulations. The system entropy as a function of the temperature can be obtained by numerically integrating the specific-heat curve. The integration constant  $S_0$  at zero temperature can be fixed by the fact that the high- $T$  entropy density of the Potts model should approach  $\ln 4$ . As shown in Fig. 3(b), the numerically determined residual entropy  $S_0/Nk_B \approx 0.2112$  agrees very well with the Pauling estimate.

*Emergent Coulomb phase.* Although the Potts ground state is disordered, the local hard constraints give rise to nontrivial long-range correlations, similar to the case in dimer models [17] and spin ice [18, 19]. To make manifest the analogy with frustrated spin systems, we consider a Heisenberg antiferromagnet in the pyrochlore lattice:

$$H = J' \sum_{\langle ml \rangle} \mathbf{S}_m \cdot \mathbf{S}_l + D \sum_m f(\mathbf{S}_m; \{\boldsymbol{\tau}_\nu\}). \quad (6)$$

Here  $J' = 3J/4$  and  $\mathbf{S}_m$  denotes a classical  $O(3)$  vector of unit length. The second term represents a special ‘tetrahedral’ anisotropy: the function  $f(\mathbf{S})$  has four degenerate minimum at the tetrahedral vectors  $\boldsymbol{\tau}_\nu$ . In the  $D \rightarrow \infty$  limit, Hamiltonian (6) reduces to the Potts model as the spins are aligned to the tetrahedral vectors according to  $\mathbf{S}_m = \boldsymbol{\tau}_{\sigma_m}$ . Moreover, since the exchange term in (6) can be rewritten as  $(J'/2) \sum_{\boxtimes} |\mathbf{S}_{\boxtimes}|^2$ , where  $\mathbf{S}_{\boxtimes}$  denotes the total spin of a tetrahedron, a Potts configuration that satisfies the 4-color constraint thus maps to a ground state of the spin model as  $\mathbf{S}_{\boxtimes} = \sum_{\nu=0}^3 \boldsymbol{\tau}_\nu = 0$ .

The mapping to Heisenberg spins also allows us to recast the color constraint into a conservation law of effective magnetic flux [18–20]. We first define three ‘magnetic’ fields, each corresponds to a component of the Heisenberg spin, at the diamond sites:

$$\mathbf{B}^\alpha(\mathbf{r}_i) = \sum_{\nu=0}^3 S_{ij}^\alpha \hat{\mathbf{n}}_\nu = \sum_{\nu=0}^3 \tau_{\sigma_m}^\alpha \hat{\mathbf{n}}_\nu. \quad (7)$$

Here  $\alpha = x, y, z$  and the pyrochlore site  $m$  corresponds to the bond  $\langle ij \rangle \parallel \hat{\mathbf{n}}_\nu$  in the diamond lattice, *i.e.*  $\mathbf{S}_{ij} = \mathbf{S}_m$ . In the coarse-grained approximation, the color constraints  $\mathbf{S}_{\boxtimes} = 0$  translate to a divergence constraint  $\nabla \cdot \mathbf{B}^\alpha(\mathbf{r}) = 0$  for the magnetic fields.

The effective free energy of the ground-state manifold arises entirely from entropy and has the form of the magnetostatic theory with three independent flux fields  $F[\mathbf{B}^\alpha(\mathbf{r})] \propto \sum_\alpha \int d^3\mathbf{r} |\mathbf{B}^\alpha(\mathbf{r})|^2$ . Essentially, it states that the partition function is dominated by microstates characterized by  $\mathbf{B}^\alpha \approx 0$ . This is due to a large number of flippable loops in such states. Although superficially  $F$  describes Gaussian fluctuations of the magnetic fields, the divergence-free constraint in momentum space  $\mathbf{k} \cdot \mathbf{B}^\alpha(\mathbf{k}) = 0$  indicates that only transverse fluctuations are allowed. Consequently, the correct correlators are obtained by projecting out the longitudinal fluctuations.

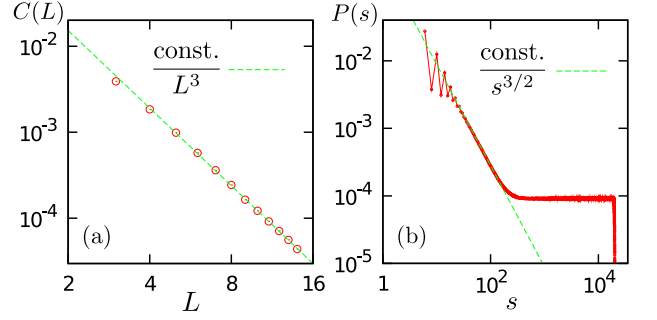


FIG. 4: (Color online) (a) Correlation function vs linear system size  $L$  from Monte Carlo simulations. Here  $C(L)$  denotes the color correlation between two points separated by  $(L/2, L/2, 0)$  in a finite lattice containing  $L^3$  cubic unit cells. (b) The length distribution  $P(s)$  of flippable loops from Monte Carlo simulations on a  $L = 12$  system.

The asymptotic field correlators in real-space has the famous dipolar form

$$\langle B_a^\alpha(\mathbf{r}) B_b^\beta(0) \rangle \propto \delta_{\alpha\beta} (\delta_{ab} - 3\hat{r}_a \hat{r}_b) / r^3 \quad (8)$$

characteristic of a Coulomb phase [21].

We also performed Monte Carlo simulations to investigate the color correlators at large distances. Fig. 4(a) shows the correlation function  $C(L)$  between two sites separated by  $\mathbf{r} = \frac{L}{2}(1, 1, 0)$  as a function of the linear system size  $L$ . A power-law dependence  $C(L) \sim L^{-3}$  at large  $L$  confirms the emergence of the Coulomb phase in the Potts model. Given its critical nature, flippable loops (with alternating colors) of all sizes are expected to exist in the Coulomb phase. In numerical simulations, however, the largest loop is bounded by the system size. Fig. 4(b) shows the length distribution  $P(s)$  of loops from Monte Carlo simulations. Similar to those found in the Coulomb phase of spin ice [22], the distribution exhibits two regimes with distinct behaviors. For short loops, the probability function scales as  $P(s) \sim s^{-3/2}$ , while an  $s$ -independent regime is observed for larger  $s$ .

In terms of the flux fields, the orbital angular momentum can be expressed as  $\mathbf{L} = \mathbf{B}^\alpha \times \mathbf{B}^\beta$ , where the two components  $\alpha \neq \beta$  depend on the particular mapping between phases and colors. The correlation function of angular momentum thus exhibits a power-law  $1/r^6$  decay in the degenerate manifold.

*Mapping for  $\Delta U > 0$ .* At last, if we take  $\Delta U$  as a free variable and consider the situation of  $\Delta U > 0$ , the classic ground states are also described by the 4-coloring model but with a different mapping. For each site  $i$ , the particle density in the three  $p$ -orbitals are equal in order to minimize the term of  $\Delta U$ , thus its angular momentum  $\mathbf{L}_i$  is parallel or anti-parallel to one of the four bond directions. Such a bond is the nodal line of the onsite condensate, thus it is broken as marked by  $\mathbf{Y}$ . The kinetic energy of any of the other three bonds  $\langle ij \rangle$  becomes  $E_{ij} = -\frac{8}{9}nt_{\parallel} \cos(\phi_{i,\nu} - \phi_{j,\nu})$  where  $\langle ij \rangle \parallel \hat{\mathbf{n}}_\nu$ .

Again  $\phi_{i,\nu}$  can be decomposed as  $\phi_{i,\nu} = \theta_i + \frac{2}{3}\sigma_{ij}\pi$ , where  $\sigma_{ij} = 0, 1, 2$  are the color indices (marked as  $\mathbf{R}$ ,  $\mathbf{G}$ ,  $\mathbf{B}$ , respectively). The even and odd permutations of the 3 colors determines whether  $\mathbf{L}_i \parallel \hat{\mathbf{n}}_\nu$  or  $-\hat{\mathbf{n}}_\nu$ . The 24 coloring patterns for the four bonds connecting to site  $i$  is classified as 8 different chiralities, and for each chirality there are 3 configurations corresponding to a  $C_3$  rotation around  $\mathbf{L}_i$ .

*Conclusion.* We have studied a diamond-lattice four-coloring model which describes the frustrated couplings between the superfluid phase degrees of freedom for  $p$ -band Bose-Einstein condensates in the diamond lattice. We have also shown that the ground states of the 4-coloring model is macroscopically degenerate and is described by an effective magnetostatics theory with three independent flux fields. Both color and orbital angular momentum correlations decay algebraically in this emergent Coulomb phase. Interestingly, point defects violating the color constraints carry “magnetic” charges corresponding to two of the three flux fields. A future direction of study is to explore the kinematics and dynamics of these novel quasiparticles. Finally, another challenging task is to examine how the huge degeneracy is lifted through quantum order-by-disorder mechanism.

*Acknowledgment.* We thank useful discussions with R. Moessner. G.W.C. acknowledges the support of ICAM and NSF Grant DMR-0844115. C.W. is supported by the NSF DMR-1105945 and the AFOSR-YIP program.

*Note added.* Upon completion of this work, we became aware of similar results on the pyrochlore 4-state Potts model in Ref. [23].

---

[1] V. F. Petrenko and R. W. Whitworth, *Physics of ice* (Oxford, New York, 1999).

- [2] see S. T. Bramwell and M. J. P. Gingras, *Science* **294**, 1495 (2001); C. Castelnovo, R. Moessner, S. L. Sondhi, *Annu. Rev. Condens. Matter Phys.* **3**, 35 (2012).
- [3] N. Shannon, O. Sikora, F. Pollmann, K. Penc, P. Fulde, *Phys. Rev. Lett.* **108**, 067204 (2012).
- [4] G.-W. Chern and C. Wu, *Phys. Rev. E* **84**, 061127 (2011).
- [5] R. Moessner, A. P. Ramirez, *Phys. Today* **59**, 24 (2006).
- [6] C. Wu, *Phys. Rev. Lett.* **100**, 200406 (2008).
- [7] E. Zhao, W. V. Liu, *Phys. Rev. Lett.* **100**, 160403 (2008).
- [8] P. Hauke, E. Zhao, K. Goyal, I. H. Deutsch, W. V. Liu, M. Lewenstein, *Phys. Rev. A* **84**, 051603(R) (2011).
- [9] C. Wu, *Mod. Phys. Lett.* **23**, 1 (2009).
- [10] Similar physics has also been studied in Josephson junction arrays of unconventional superconductors, see, e.g. J. E. Moore, D.-H. Lee, *Phys. Rev. B* **69**, 104511 (2004); C. Xu, J. E. Moore, *Nucl. Phys. B* **716**, 487 (2005).
- [11] R. P. Feynman, *Statistical Mechanics*, (Addison-Wesley Publishing Company, 1972).
- [12] M. Oelschlaeger, G. Wirth, A. Hemmerich, *Phys. Rev. Lett.* **106**, 015302 (2011); G. Wirth, M. Oelschlaeger, A. Hemmerich, *Nature Phys.* **7**, 147 (2011).
- [13] R. J. Baxter, *J. Math. Phys.* **11**, 784 (1970).
- [14] J. Kondev, C. L. Henley, *Phys. Rev. B* **52**, 6628 (1995).
- [15] O. Toader, T. Y. M. Chan, and S. John, *Phys. Rev. Lett.* **92**, 043905 (2004).
- [16] W. V. Liu, and C. Wu, *Phys. Rev. A* **74**, 13607 (2006).
- [17] D. A. Huse, W. Krauth, R. Moessner, and S. L. Sondhi, *Phys. Rev. Lett.* **91**, 167004 (2003).
- [18] S. V. Isakov, K. Gregor, R. Moessner, and S. L. Sondhi, *Phys. Rev. Lett.* **93**, 167204 (2004).
- [19] C. L. Henley, *Phys. Rev. B* **71**, 014424 (2005).
- [20] M. Hermele, M. P. A. Fisher, and L. Balents, *Phys. Rev. B* **69**, 064404 (2004).
- [21] C. L. Henley, *Annu. Rev. Condens. Matter Phys.* **1**, 179 (2010).
- [22] L. D. C. Jaubert, M. Haque, and R. Moessner, *Phys. Rev. Lett.* **107**, 177202 (2011).
- [23] V. Khemani, R. Moessner, S. A. Parameswaran, and S. L. Sondhi, arXiv:1204.3646.